Tectonophysics 866 (2023) 230041

Contents lists available at ScienceDirect

Tectonophysics

journal homepage: www.elsevier.com/locate/tecto

Characterization of the co-seismic pattern and slip distribution of the February 06, 2023, Kahramanmaraş (Turkey) earthquakes (M_w 7.7 and M_w 7.6) with a dense GNSS network

Ali Özkan [a], Halil İbrahim Solak [b,d], İbrahim Tiryakioğlu [c,d], Murat Doruk Şentürk [e], Bahadır Aktuğ [e], Cemil Gezgin [f], Fatih Poyraz [g], Hüseyin Duman [g], Frédéric Masson [h], Göksu Uslular [i], Cemal Özer Yiğit [j], Hasan Hakan Yavaşoğlu [i,k,*]

[a] Osmaniye Vocational School, Osmaniye Korkut Ata University, Osmaniye, Türkiye
[b] Distance Education Vocational School, Afyon Kocatepe University, Afyonkarahisar, Türkiye
[c] Department of Geomatics Engineering, Afyon Kocatepe University, Afyonkarahisar, Türkiye
[d] Earthquake Implementation and Research Center, Afyon Kocatepe University, Afyonkarahisar, Turkey
[e] Department of Geophysical Engineering, Ankara University, Gölbaşı, Ankara, Türkiye
[f] Department of Geomatics Engineering, Aksaray University, Aksaray, Türkiye
[g] Department of Geomatics Engineering, Sivas Cumhuriyet University, Sivas, Türkiye
[h] Institut Terre et Environnement de Strasbourg (ITES), UMR7063, Université de Strasbourg/EOST CNRS, Strasbourg, France
[i] TÜBİTAK Marmara Research Center, Polar Research Institute, Gebze, Türkiye
[j] Department of Geomatics Engineering, Gebze Technical University, Gebze, Türkiye
[k] Department of Geomatics Engineering, Istanbul Technical University, Istanbul, Türkiye

ARTICLE INFO

Keywords:
GPS
Co-seismic displacement
Slip distribution
Kahramanmaraş
East Anatolian Fault Zone

ABSTRACT

Two consecutive earthquakes with the magnitudes of M_w 7.7 and 7.6 (February 06, 2023) occurred on the East Anatolian Fault Zone (EAFZ) segments and unfortunately resulted in significant devastation to human life and cities in Turkey and Syria. In this study, we aimed to analyse the co-seismic displacements and fault slip distributions of these seismic events. Our unique high-spatial-resolution Global Navigation Satellite System (GNSS) network (comprising 73 permanent GNSS stations and 40 campaign observation sites), providing the recent geodetic dataset for the region, allows better constraint of the co-seismic surface displacements and slip distributions of both earthquakes. The three largest total displacements were identified as 466 cm, 362 cm, and 360 cm. The Fault interactions along the EAFZ were obvious during the consecutive earthquakes. The ruptures mainly occurred in the left-lateral components of the fault segments, with the maximum slips of 7.25 m and 9.43 m for the first event along the EAFZ and the second event on the Çardak Fault, respectively.

1. Introduction

The East Anatolian Fault Zone (EAFZ) is one of the major tectonic features in Anatolia that moves towards the west relative to the Eurasian plate due to the compressional behaviour of African, Sinai, and Arabian plates (Arpat and Şaroğlu, 1972; Bozkurt, 2001; Sengor et al., 1985; Şengör and Yılmaz, 1981). The sinistral strike-slip mechanism of the EAFZ and Dead Sea Fault Zone (DSFZ) together with the Cyprus Arc (CA) in southern Turkey, with the dextral strike-slip dominance along the North Anatolian Fault Zone (NAFZ) in the north, mostly accommodate the motion between the African, Sinai, Arabian, and Anatolian plates with respect to the Eurasian plate (Westaway, 2003).

In recent years, geodetic networks consisting of permanent Global Navigation Satellite System (GNSS) stations and campaign observation sites have been widely used to determine interseismic deformations along the EAFZ and in the vicinity of Hatay Triple Junction (HTJ) at the northern end of the DSFZ, and also to reveal the seismic hazard for the region in terms of major earthquake potential of the main active faults (Aktug et al., 2016; Aktuğ et al., 2013; Alchalbi et al., 2010; Mahmoud et al., 2012; Meghraoui et al., 2011; Yıldız et al., 2020). More recently, Yıldız et al. (2020) argued that the strike-slip rate along the sinistral main branch of the EAFZ, specifically on the Türkoğlu-Gölbaşı segment,

* Corresponding author at: TÜBİTAK Marmara Research Center, Polar Research Institute, Gebze, Türkiye.
E-mail address: yavasoglu@itu.edu.tr (H.H. Yavaşoğlu).

https://doi.org/10.1016/j.tecto.2023.230041
Received 9 April 2023; Received in revised form 12 September 2023; Accepted 14 September 2023
Available online 18 September 2023

was 7.5 mm/year. They also declared that the next probable major earthquake on this segment might occur with magnitudes of M_w 7.2–7.6, if this segment entirely ruptures over its total length of 90 km. In the same study, based on the estimations for strain accumulation ranging from 0.65 m to 1.70 m, the subsequent probable major earthquakes on the Karataş-Osmaniye Fault (KOF) and Karasu Fault (KF) segments (Fig. 1) were predicted with the magnitudes of M_w 6.8–7.2. In addition, the co-seismic displacements caused by the large earthquakes in Turkey were precisely determined with the help of high-spatial-resolution GNSS networks in recent studies (Tiryakioğlu et al., 2018; Tiryakioglu et al., 2017a, 2017b).

On February 06, 2023, the two devastating earthquakes occurred within 9 h (01.17 and 10.24, UTC Time) at epicentres in Pazarcık and Elbistan (Kahramanmaraş) with magnitudes of M_w 7.7 and 7.6, respectively (AFAD, 2023; KOERI, 2023) (Fig. 1). Unfortunately, these consecutive earthquakes caused a massive disaster in the region and devastated cities in Turkey and Syria. The preliminary studies revealed that these earthquakes had ruptured along 350 km and 160 km, respectively (Melgar et al., 2023). As of March 15, 2023, more than fifteen thousand aftershocks were recorded (KOERI, 2023).

In this study, our goal was to determine the co-seismic pattern and slip distribution of these devastating earthquakes. Using our dense GNSS network consisting of 73 permanent GNSS stations and 40 campaign observation sites, it was possible to precisely constrain the co-seismic surface displacements through inverse modelling.

2. Tectonic setting and seismotectonic characteristics of the EAFZ

The collision between the Arabian and Eurasian plates along the Bitlis-Zagros suture zone in the mid-late Miocene resulted in the formation of the EAFZ (Şengör and Yılmaz, 1981). Despite the debate about the time of transition between compressional and transtensional tectonism in the region (e.g., ~11 Ma, Sengor et al., 1985; ~3 Ma, Faccenna et al., 2006; Hubert-Ferrari et al., 2009; Westaway and Arger, 1996), the main neotectonic feature of the EAFZ (Fig. 1) is a left-lateral strike-slip fault with a NE-SW trend, extending at least 500 km along the Anatolian, Sinai, Arabian, and Eurasian plate boundaries (Aktug et al., 2016; Arpat and Şaroğlu, 1972; Bulut et al., 2012; Duman and Emre, 2013; Lyberis et al., 1992; Reilinger et al., 1997; Sengor et al., 1985; Taymaz et al.,

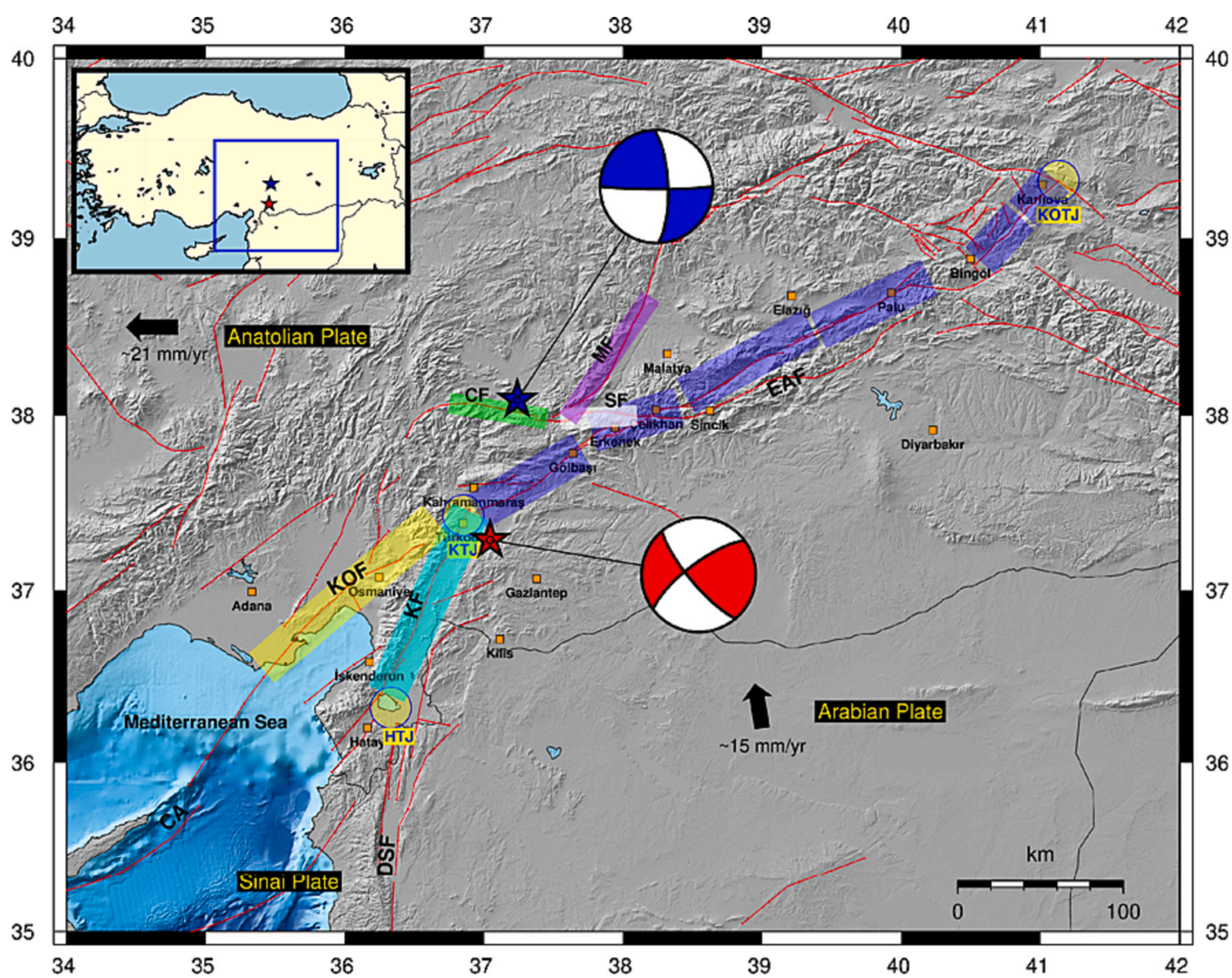

Fig. 1. The map for the study region shows fault segments with coloured stripes and the epicentres of the February 6th, 2023 Kahramanmaraş earthquakes (red star and beach ball for the first event at 01.17 UTC Time, blue star and beach ball for the second event at 10.24 UTC Time). Abbreviations are HTJ: Hatay Triple Junction; KTJ: Kahramanmaraş Triple Junction; KOTJ: Karlıova Triple Junction; EAF: East Anatolian Fault (blue stripes); DSF: Dead Sea Fault; KOF: Karataş-Osmaniye Fault (yellow stripe); CA: Cyprus Arc; KF: Karasu Fault (cyan stripe); CF: Çardak Fault (green stripe); SF: Sürgü Fault (white stripe), MF: Malatya Fault (purple stripe). Faults in red are mapped from GEM GAF-DB (Styron and Pagani, 2020). Black arrows representing the plate velocities are provided by Reilinger et al. (2006). Focal mechanism solutions were obtained from the AFAD (Disaster and Emergency Management Presidency) earthquake catalogue. (For interpretation of the references to colour in this figure legend, the reader is referred to the web version of this article.)

1991; Westaway, 2003).

The changes in geodynamic processes (e.g., tectonic regime, crustal deformation) since mid-late Miocene mostly shaped the tectonic features of the EAFZ (Dewey et al., 1986; Duman and Emre, 2013; Kiratzi, 1993; Koçyiğit et al., 2001; Mahmoud et al., 2012; Tatar et al., 2004). The EAFZ is juxtaposed with the NAFZ at Karlıova Triple Junction (KOTJ; Fig. 1), but there is still no consensus about its southwestern end. There are three different claims related to this subject: the relatively earlier studies assert that the EAFZ continues directly through the Cyprus Arc (Bozkurt, 2001; Koçyiğit et al., 2001; Taymaz et al., 1991; Westaway, 1994); other studies suggest that Kahramanmaraş (near Türkoğlu, Fig. 1) is a triple junction (KTJ) (Barka and Kadinsky-Cade, 1988; Gülen et al., 1987); while a more southern continuation of the EAFZ, where it meets with the DSFZ at HTJ, was also suggested (Alp et al., 2011; Duman and Emre, 2013; Karig and Kozlu, 1990; Saroglu et al., 1992; Şengör et al., 2018; Yıldız et al., 2020).

The EAFZ is divided into different segments along a main sinistral strike-slip component (Arpat and Şaroğlu, 1972; Barka and Kadinsky-Cade, 1988; Duman and Emre, 2013). There are also different assertions about the number of segments, but here the recent study of Duman and Emre (2013) is followed, which is mostly based on field observations, for consistency throughout the manuscript in referring to segments and strands along the EAFZ (Fig. 1). The Karlıova, Ilıca, Palu, Pütürge, Erkenek, Pazarcık, and Amanos segments along NE-SW direction constitute the main strand of the EAFZ, while the Sürgü, Çardak and Savrun segments are along the northern strand (Duman and Emre, 2013).

Many destructive historical earthquakes ($M_s \geq 6.0$) were recorded in the vicinity of EAFZ (Fig. 2). A substantial number of these earthquakes caused great devastation in southern Turkey and northern Syria. When these historical records are examined, the November 29, 1114 earthquake (M_s 6.9, Ambraseys, 2009; $M_s \geq 7.8$, Ambraseys and Jackson, 1998; M_s 7.7, Sbeinati et al., 2005) associated with the Türkoğlu-Gölbaşı segment is noteworthy. Similarly, the 1513 earthquake (M_s 7.4) is proposed to have occurred on the KOF (Fig. 2) located southwest of Türkoğlu (Ambraseys, 2009, 1989). Apart from these, two major

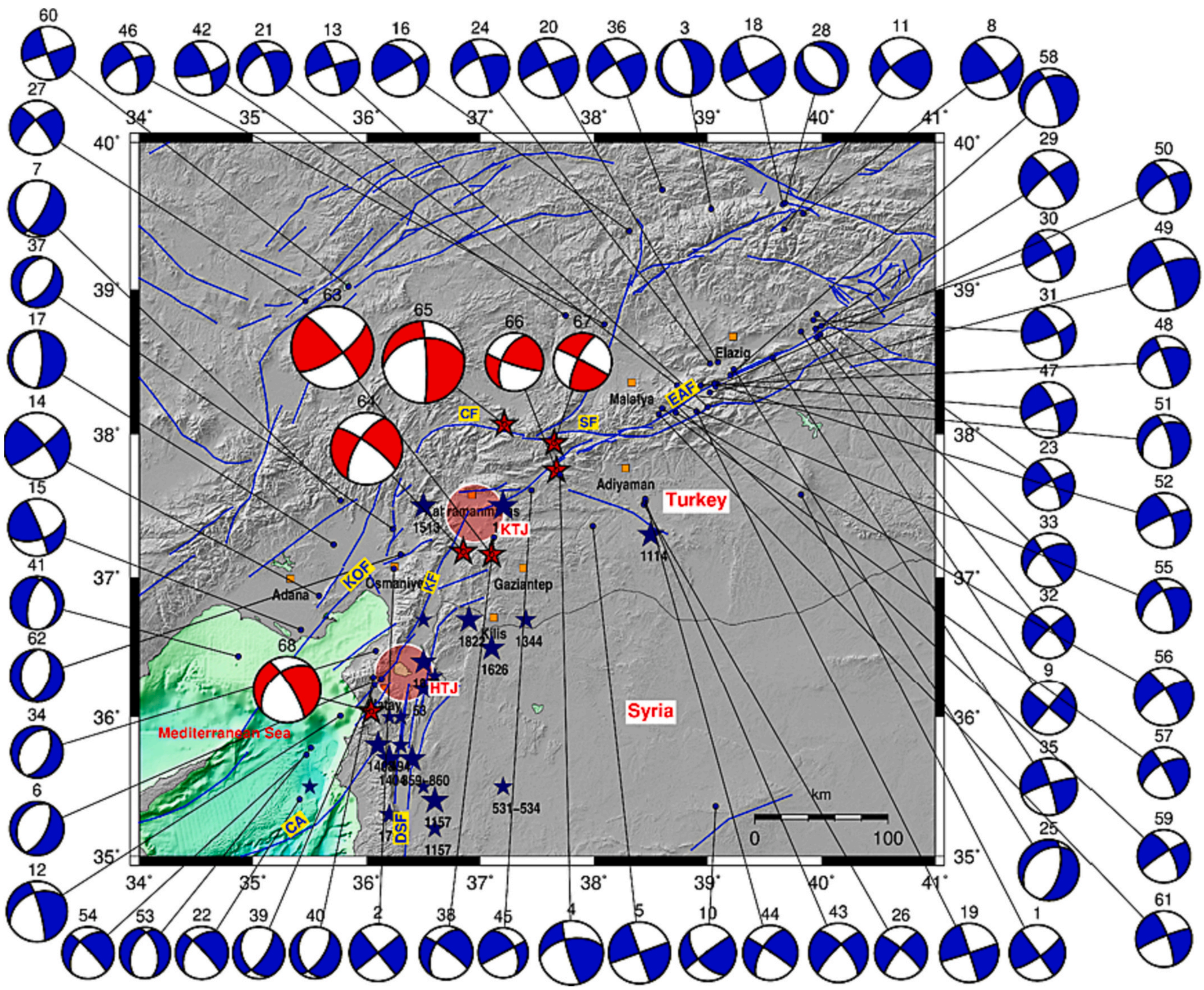

Fig. 2. Seismotectonic map of southern Turkey. Blue dots show the epicentres of the instrumental earthquakes from 01/01/1976 to 06/02/2023 and red stars represent the epicentres of the recent earthquakes that occurred within 3 weeks after February 6th, 2023 Kahramanmaraş earthquakes (All instrumental earthquakes with magnitudes of Mw ≥ 4.5 have focal mechanism solutions here). Blue starsrepresent the historical earthquakes in the region. For the details and numbering of instrumental earthquakes, see Table S1. The focal mechanism solutions and the earthquake epicentres were obtained from the Global Centroid-Moment-Tensor (CMT) Catalogue, 2023. Abbreviations are the same as in Fig. 1. (For interpretation of the references to colour in this figure legend, the reader is referred to the web version of this article.)

earthquakes affecting Hatay and its surroundings in the recent past were the August 13, 1822 (M_s 7.4) and April 3, 1872 (M_s 7.2) tremors (Ambraseys, 2009, 2006, 1989; Ambraseys and Jackson, 1998; Sbeinati et al., 2005). During the instrumental earthquake period in the region, several major earthquakes with various depths were recorded (Ambraseys, 1989; Hubert-Ferrari et al., 2020) (Figs. 2 and 3): May 22, 1971, Bingöl (M_W 6.8, KOERI); May 1, 2003, Bingöl (M_W 6.4, KOERI & M_W 6.4, USGS); March 8, 2010, Elazığ, Kovancılar (M_W 6.1, KOERI & USGS), and January 24, 2020, Elazığ, Sivrice (M_W 6.5, KOERI & M_W 6.7, USGS). Accordingly, apart from some exceptional cases, it can be argued that the main faults in southern Turkey, particularly the EAFZ, have predominantly strike-slip mechanisms that cause significant seismic activity in the region. However, there are also some earthquakes that occurred due to normal faulting (e.g., earthquakes labelled 34, 37 and 62 in Table S1 and Fig. 2) in the vicinity of KOF and KF. This indicates the faulting pattern and the features of the tectonic mechanism along different segments in Kahramanmaraş and the surrounding region.

2.1. *February 6th, 2023, Kahramanmaraş Earthquakes*

On February 06, 2023, two major earthquakes occurred in districts of Kahramanmaraş (Pazarcık and Elbistan) with magnitudes of M_W 7.7 and 7.6, respectively (AFAD, 2023; KOERI, 2023; Fig. 3). The first earthquake (Pazarcık) coincided with the Narlı segment at the northern end of the DSFZ around Karasu Rift (Rojay et al., 2001; Tatar et al., 2004), while the second earthquake (Elbistan) was along the Çardak Segment of the northern strand of EAFZ (Figs. 1 and 2). The focal depths published by different institutions revealed that both earthquakes were shallow, with average depths of 16 km and 13 km, respectively (KOERI, 2023) (Figs. 2 and 3). The earthquakes affected the neighbouring provinces and the countryside around the epicentres, resulting in substantial destruction and extensive damage. Subsequent to the two main shocks on February 06, 2023 (at 01.17 and 10.24 UTC Time) in Kahramanmaraş, by March 15, 2023, the region witnessed approximately 318 aftershocks ($M_W \geq 4.5$) (Fig. 3, Table S2). The most pronounced of these aftershocks (M_W 6.6) occurred in Nurdağı, Gaziantep, on February 06, 2023, approximately eleven minutes after the first main shock. One of the largest aftershocks was recorded in Hatay on February 20, 2023, with magnitude of M_W 6.4 (AFAD, 2023; KOERI, 2023; Table S2).

3. Methodology

3.1. *GNSS network*

A total of 73 permanent GNSS stations and 40 campaign observation sites (Fig. 4) were used to investigate co-seismic displacements and slip distributions of the Kahramanmaraş earthquakes. The permanent stations of the Turkish National Permanent GNSS Network-Active (TUSAGA-Active) close to the epicentres of the recent devastating

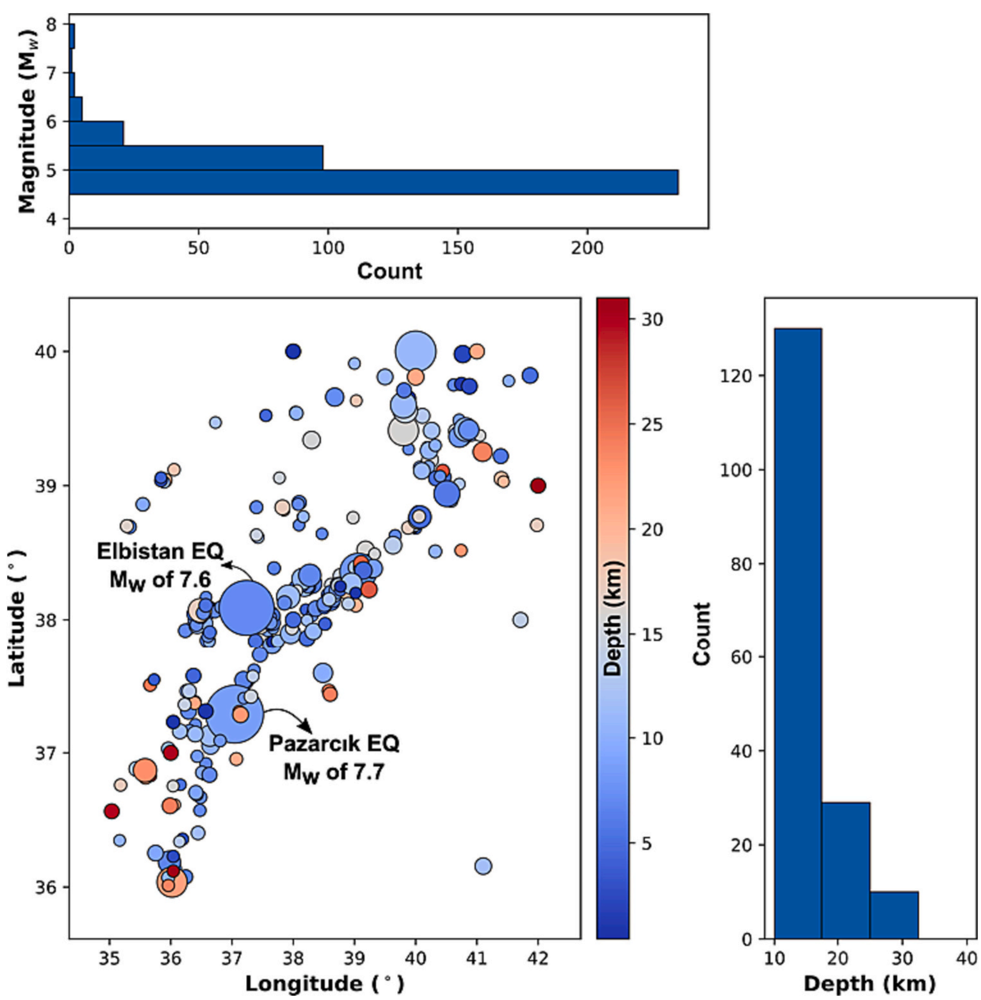

Fig. 3. Distribution and basic statistics for the instrumental earthquakes (01/01/1990–15/03/2023; AFAD and KOERI Catalogues) with magnitudes of $M_W \geq 4.5$ occurring near the Kahramanmaraş region (Table S2). The symbol size and colour represent the magnitude and focal depth of the earthquakes, respectively. The histograms display the number of earthquakes versus magnitude (M_W) and focal depth in km.

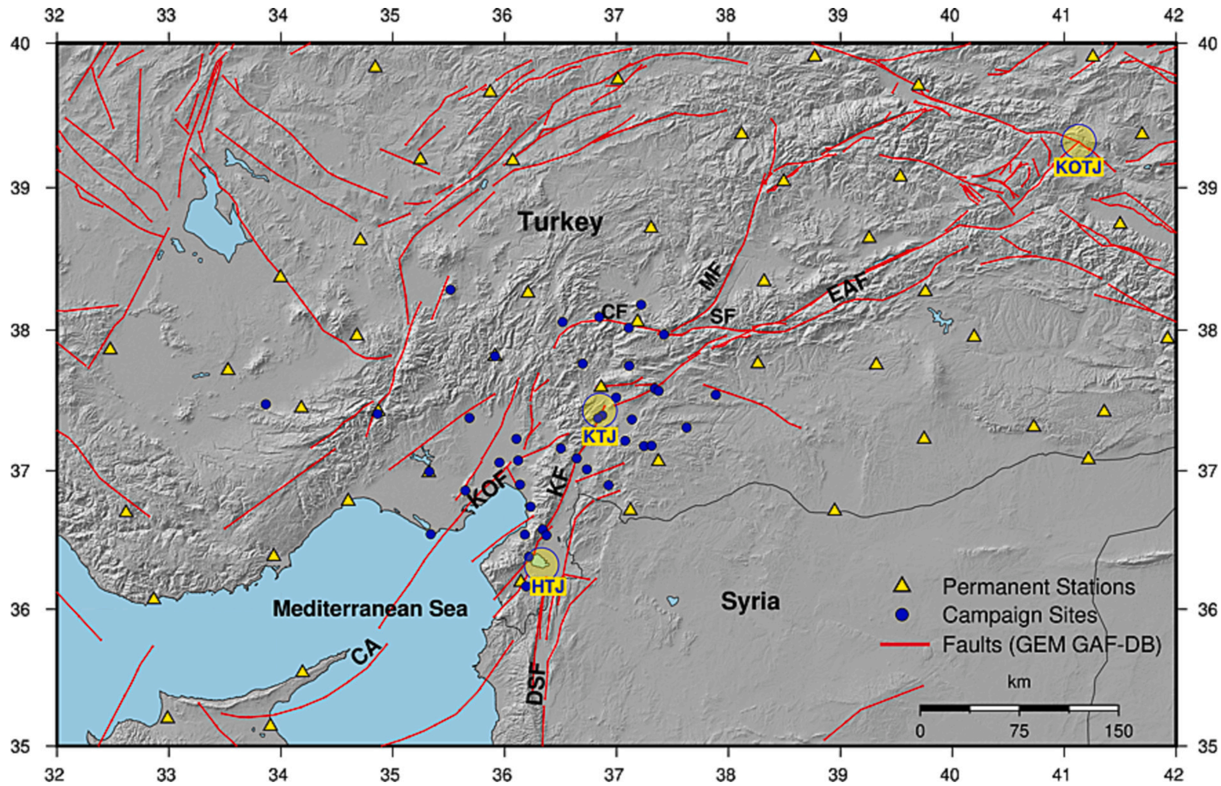

Fig. 4. The GNSS network used in this study. Yellow triangles and blue circles represent the permanent GNSS stations and campaign observation sites, respectively. Abbreviations are the same as in Fig. 1. (For interpretation of the references to colour in this figure legend, the reader is referred to the web version of this article.)

earthquakes are operated by the Ministry of National Defence (Turkey) General Directorate of Mapping and other institutions. The campaign observation sites, which were previously studied in the region (~7 km away from the first earthquake epicentre) by our team (Yıldız et al., 2020), were used here to perform GNSS measurements for six days (12–19 February 2023) after the earthquakes. In this study, the co-seismic zones with sparse site distribution were densified by integrating periodically observed Turkish National Fundamental GPS Network (TUTGA) sites (Fig. 4). The minimum 4-h static GNSS measurements were performed with the 30-s sampling rate, and the cut-off angle was 10 degrees in elevation.

3.2. Co-seismic displacement analysis

There is a close relationship between co-seismic displacements and time series models. The utilization of permanent GNSS stations is promising for devising both short-term and long-term solutions to mitigate displacement (e.g., Aktuğ et al., 2010; Tiryakioglu et al., 2017a). Evaluation of long-term time series can yield insights into the motions of a station, which may manifest as linear, periodic, irregular, or episodic behaviours.

The precise coordinates of the sites in our GNSS network before (Day of Year-DOY 036, February 05, 2023) and after (DOY 038, February 07, 2023) the Kahramanmaraş earthquakes on February 06, 2023 were calculated using the GAMIT/GLOBK software (Herring et al., 2015a, 2015b). In order to process the GNSS data using the GAMIT software, the rapid orbit product, earth rotation parameters, and absolute antenna phase centres were obtained from Scripps Orbit and Permanent Array Centre (SOPAC) (Jamason et al., 2004). Moreover, the antenna phase centres were based on the height-dependent model (Herring et al., 2015b). The FES2004 Ocean Tide Loading (OTL) grid and the ionosphere-free linear combinations (LC) of L1 and L2 carrier phases were also introduced in the GNSS data processing (Gülal et al., 2013; Herring et al., 2015b; Tiryakioğlu et al., 2013). The daily coordinates were estimated by integrating the selected International GNSS Service (IGS) stations with stable position time series as detailed in the following studies (Aktug et al., 2016; Tiryakioglu et al., 2017a; Yavasoglu et al., 2021; Yıldız et al., 2020).

The velocities obtained from a long-term time series analysis of campaign sites within the GNSS network were published by Kurt et al. (2023) and Yıldız et al. (2020). Specifically, Kurt et al. (2023) proposed a model encompassing 836 sites pertinent to the national velocity field of Turkey. This model provided the annual interseismic velocities for each respective site. Given that most of the sites within the scope of this study were long-term campaign sites, epochs were adjusted using their own velocities. The pre-earthquake coordinates of these sites were adjusted to the earthquake epoch by using the velocity of each site. This entailed scaling the velocity of each site by the temporal discrepancy between its last observation and the earthquake epoch, with the obtained values being integrated into the site coordinates. For the permanent GNSS stations, the displacements were calculated by taking the differences of the coordinates before and after the earthquakes, without any epoch adjustment.

In order to accurately determine the total co-seismic displacements that occurred with the Kahramanmaraş earthquakes, the coordinates of each observation site obtained from the daily solutions before and after the earthquakes (DOY 036 and DOY 038) were compared. The total co-seismic displacements from the short-term solutions were determined using Eq. (1).

$$\Delta e\_cos = e\_38 - e\_36; \Delta n\_cos = n\_38 - n\_36; \Delta h\_cos = h\_38 - h\_36 \quad (1)$$

where Δe_cos, Δn_cos, Δh_cos are the total co-seismic displacements for each component, e_36, n_36, h_36 and e_38, n_38, and h_38 denote the positions estimated from GNSS solutions for DOY 036 and 038, respectively. The co-seismic displacement time series were derived within the reference frame of ITRF2014. The uncertainties associated with the coordinate differences were calculated using standard error propagation considering the uncertainties of the east and north horizontal position components estimated based on GNSS observations before and after the earthquakes (Table S3).

3.3. Inversion

The GNSS-derived co-seismic displacements were modelled as the surface displacements of a finite dislocation in an elastic half-space (Okada, 1985). The relationship between surface displacements and fault geometry parameters is inherently nonlinear, characterized by numerous local minima. In order to invert the displacements for the fault geometry and slip rates, a hybrid optimization scheme was adopted involving global and local optimization. The details of the optimization strategy can be found in Aktuğ et al. (2010). The objective function was the Weighted Residual Sum of Squares (WRSS) between the observed and the modelled displacements. The main advantage of employing this hybrid approach lies in its capability to avoid local minima while simultaneously providing an efficient solution. A two-step approach was followed for the inversion (Aktuğ et al., 2010). Initially, an inversion of the co-seismic displacements was performed to derive the fault geometry, whereby a homogeneous slip distribution was assumed over the initial fault model. The subsequent phase was dedicated to estimation of the slip components with fixed fault geometry ascertained from the first step.

Since the fault geometry parameters are non-linear with respect to the surface displacements, the inversion of the fault geometry requires meticulous consideration. The algorithm for the inversion method should be able to reach the global minimum while concurrently producing efficient estimations. To this end, we employed the Simulated Annealing method (Kirkpatrick et al., 1983), which is a global optimization scheme adapted to avoid local minima. While global optimization methods can reach global minima, they often lack the efficiency of quasi-Newton methods in proximity to these minima. Therefore, after obtaining parameters in the vicinity of global minimum, the parameters were further refined by utilizing the Boyden-Fletcher-Goldfarb-Shanno (BFGS) algorithm.

Snow cover partially allows for the use of satellite radar observations for the determination of the rupture. Hence, most of the apriori fault geometry and rupture are sourced from on-site geological field observations of the rupture. The USGS (USGS, 2023a, 2023b) provided a set of six-segment fault geometry, which was employed as apriori in our inversion (Fig. S3). The geometry resulting from the inversion closely aligns with the apriori model.

The average interstation distance for the permanent stations within the TUSAGA-Active network is ~100 km, which provides a relatively low spatial resolution. However, the campaign GNSS observations provide saturation-free near-field data to resolve the geometry and the slips for the Kahramanmaraş earthquakes. In fact, one of the main advantages of the seismogeodetic GNSS observations is that it is saturation-free even at the closest distances to the rupture enabling better capture of the co-seismic deformation pattern. Contrary to this, seismic sensors such as seismometers and accelerometers may be weak in detecting larger magnitudes with more energy at low frequencies. This might cause the magnitude of the earthquake to be underestimated or saturated. The obtained parameters are given below in Table 1.

After inverting the fault geometry and unit slips in the first step, the observed displacements were inverted for the individual slips by solving the equation using the elastostatic green functions given in Okada (1985).

$$\begin{bmatrix} u \\ 0 \\ 0 \end{bmatrix} = \begin{bmatrix} G_{ss} & G_{ds} \\ \kappa L & 0 \\ 0 & \kappa L \end{bmatrix} \begin{bmatrix} S_{ss} \\ S_{ds} \end{bmatrix} \tag{2}$$

where G, u, κ and L are green functions which relate the slip components to the surface displacements, the observed surface displacements, the smoothing constant and the finite-difference approximation of the Laplacian operator. The Laplacian operator serves as a dual purpose: it constrains the slip rate variations along both the strike and the dip directions and stabilizes the underdetermined linear systems of equations. While Eq. (2) can also be solved by the simple least squares method, it is necessary to ensure non-negativity for the slips. A quasi-Newton optimization scheme was applied, incorporating constraints to prevent the back-slip on individual patches. The patch size of 6 km was selected. The slip distributions on the fault planes were estimated using a constrained optimization scheme (Wang et al., 2009). Using the inverted fault geometry, a distributed slip model was obtained by the steepest descent method. For the slip distribution, SDM software (Wang et al., 2009) was used, which utilizes Modified Lanczos Inverse. This methodology ascertains a model proximate to one with minimum roughness.

4. Results

The horizontal co-seismic surface displacements were calculated for the earthquake series in Kahramanmaraş, Turkey using our dense GNSS network (Fig. 4, Table S3). The inversion was carried out by using 3D measurements, including vertical displacements. However, the horizontal displacements were 10–40 times larger than the vertical displacements even at the closest sites to the earthquake epicentres (Figs. S5–S7), and about 5 times noisier than the horizontal components. Therefore, the vertical co-seismic offsets were automatically de-weighted in the inversion according to their covariance and the inversion results were dominated by the horizontal co-seismic displacements. The co-seismic displacements decomposed into the east (E) and north (N) components at the selected permanent GNSS stations were illustrated in Fig. 5. Starting from 10 days before the earthquakes, the time series were derived by processing the data of a minimum of 20 days at all permanent stations considering the data availability. The maximum total co-seismic displacements for the E and N components individually were 4638 ± 3 mm and 2765 ± 4 mm at the EKZ1 and FEVZ sites, respectively (Fig. 5, Table S3). The total co-seismic displacement varies at different sites (≥1 m at 17 sites, ≥50 cm at 13 sites, ≥10 cm at 12 sites, and <10 cm at 71 sites) (Figs. S1, S2, and S3).

The closest sites to the first earthquake epicentre were SRLR (~12 km) and BOYN (~13 km). The recorded co-seismic displacements for the E components at these sites (SRLR and BOYN) were 704 ± 6 mm and 501 ± 6 mm, while the N components were 964 ± 5 mm and 554 ± 6 mm, respectively. However, the FEVZ site, situated ~42 km west of the

Table 1
The obtained geometry and slip parameters along the fault segments (1–6).

Segment number	Lon.[a] (°)	Lat.[a] (°)	Strike (°)	Depth (km)	Dip (°)	Length (km)	Left-lateral slip (m)	Reverse slip (m)[b]
1	37.0791	37.25	33.01	10.42	80.15	45.32	1.52	1.41
2	36.6656	37.31	59.90	18.27	85.02	169.85	4.94	−0.29
3	36.1031	36.16	24.91	13.89	88.14	149.34	3.73	0.11
4	37.5570	37.96	−82.91	9.85	89.62	85.20	3.91	−1.41
5	36.8301	38.09	−104.81	9.66	86.89	30.24	0.72	1.49
6	37.6020	37.99	54.82	15.47	82.63	85.02	4.07	−0.52

[a] Starting position of the segment.
[b] Negative values correspond to normal slip.

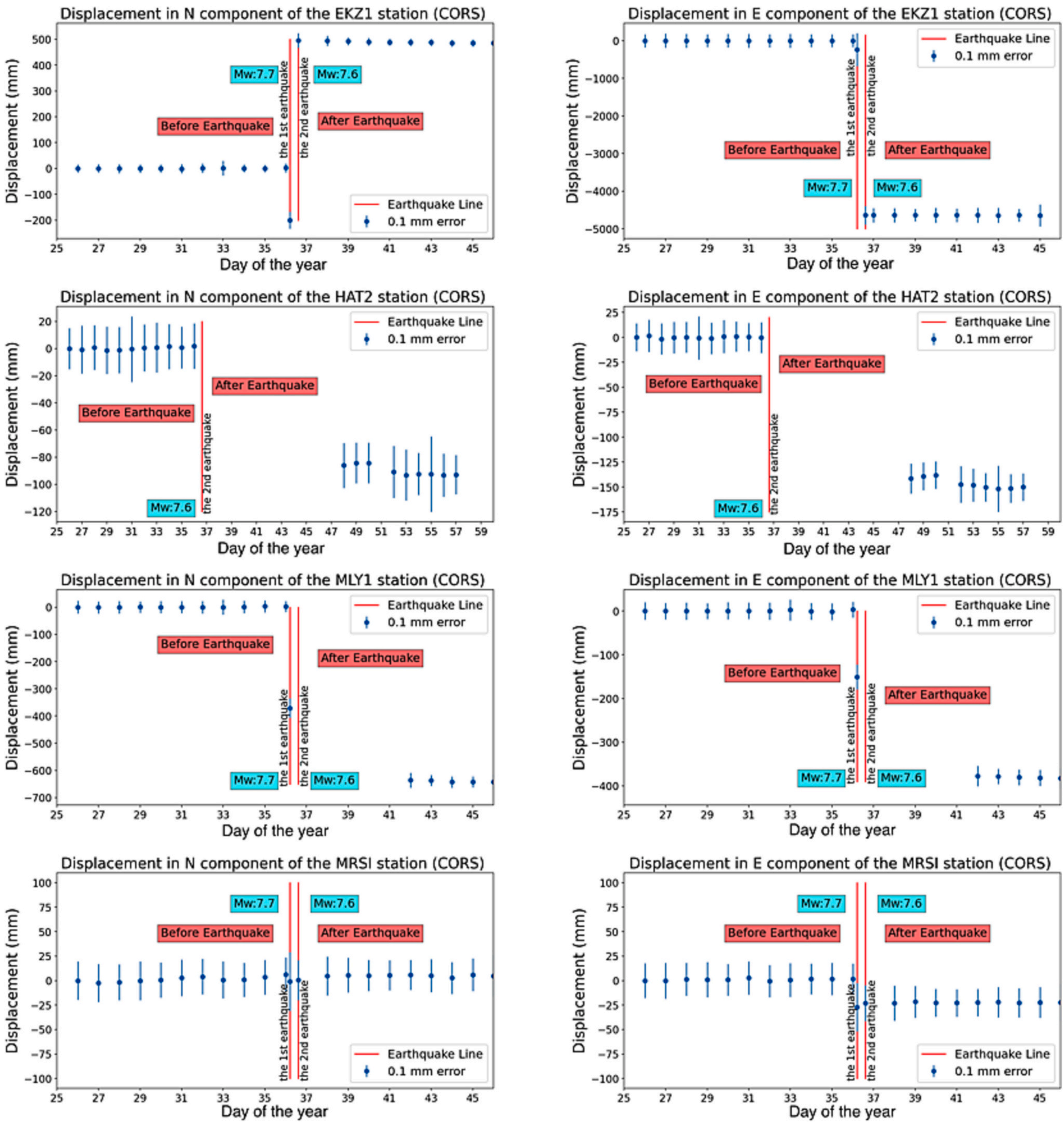

Fig. 5. The co-seismic displacements at the selected permanent GNSS stations (EKZ1, HAT2, MLY1, and MRSI) caused by the recent Kahramanmaraş earthquakes. For each row, the left and right figures represent the displacements on the north and east components at each station, respectively.

epicentre (Fig. 4) and within the seismic zone of the first earthquake, exhibited a total co-seismic displacement of 1028 ± 4 mm and 2765 ± 4 mm for the E and N components, respectively.

The closest sites to the second earthquake epicentre, which were EKZ1 (~7 km) and KAND (~15 km) (Fig. 4), experienced larger offsets. The total co-seismic displacements at the EKZ1 and KAND sites were 4638 ± 2 mm and 2160 ± 7 mm on the E components and 496 ± 3 and 1019 ± 11 mm on the N components, respectively (Fig. 5, Table S3). Additionally, the total co-seismic displacements on the E components at the MLY1 and HAT2 sites were 381 ± 2 mm and 141 ± 2 mm, respectively. However, the N component displacement at the MLY1 site was 638 ± 2 mm, while it was only 88 ± 2 mm at the HAT2 site (Fig. 5, Table S3).

The goodness-of-fit of our inversion model was validated through a comparison between the observed and modelled co-seismic displacements (Fig. 6). The total magnitude of the two major earthquakes that occurred within 9 h was calculated as M_w 8.0.

The slip distribution demonstrates very high concentration along the whole Segment-2, Segment-3, Segment-4 and Segment-6 (Figs. 7 and S3). The maximum slips were observed in Segment-4 and Segment-2 of 9.43 m and 7.25 m, respectively. As opposed to the slips on the other segments, the slips were shallower in Segment-5. Given that our co-seismic dataset encompasses both earthquakes, the co-seismic displacements at the permanent GNSS stations were used to obtain the

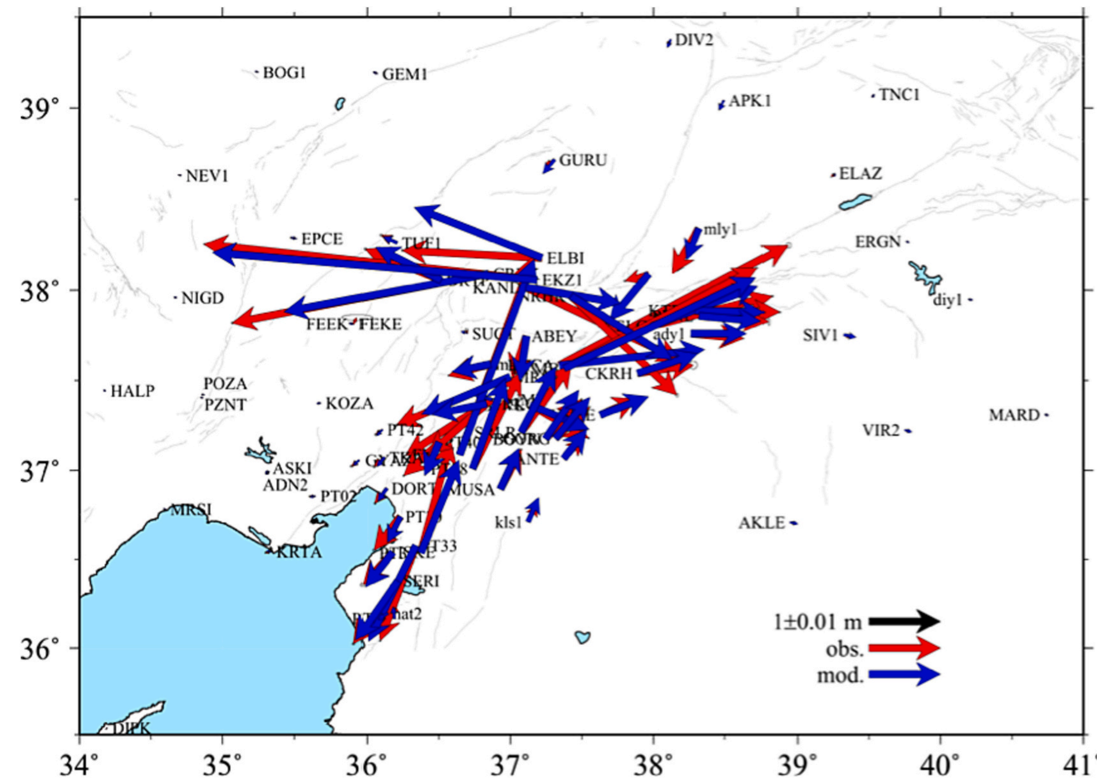

Fig. 6. The finite source model with the distributed slips obtained from the inversion of the observed displacements. Error ellipses are at 95% confidence level.

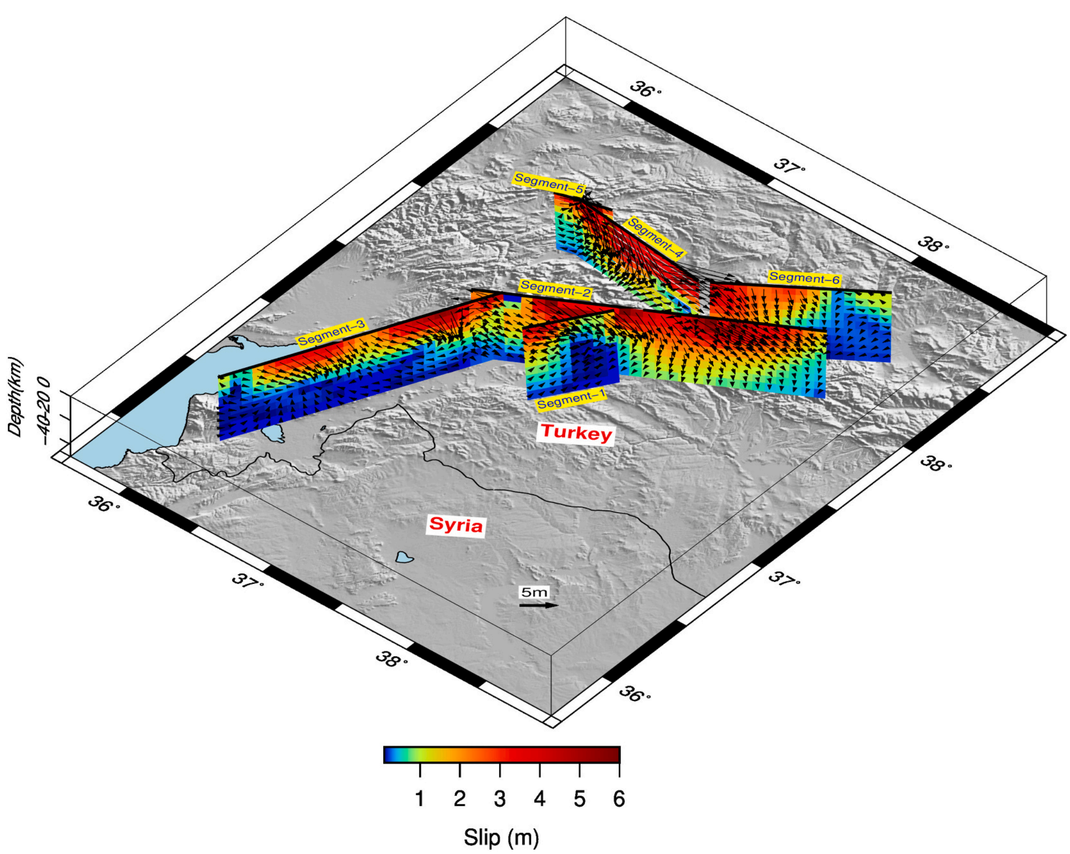

Fig. 7. The slip distributions with their directions calculated using the co-seismic displacements of two consecutive earthquakes on February 06, 2023.

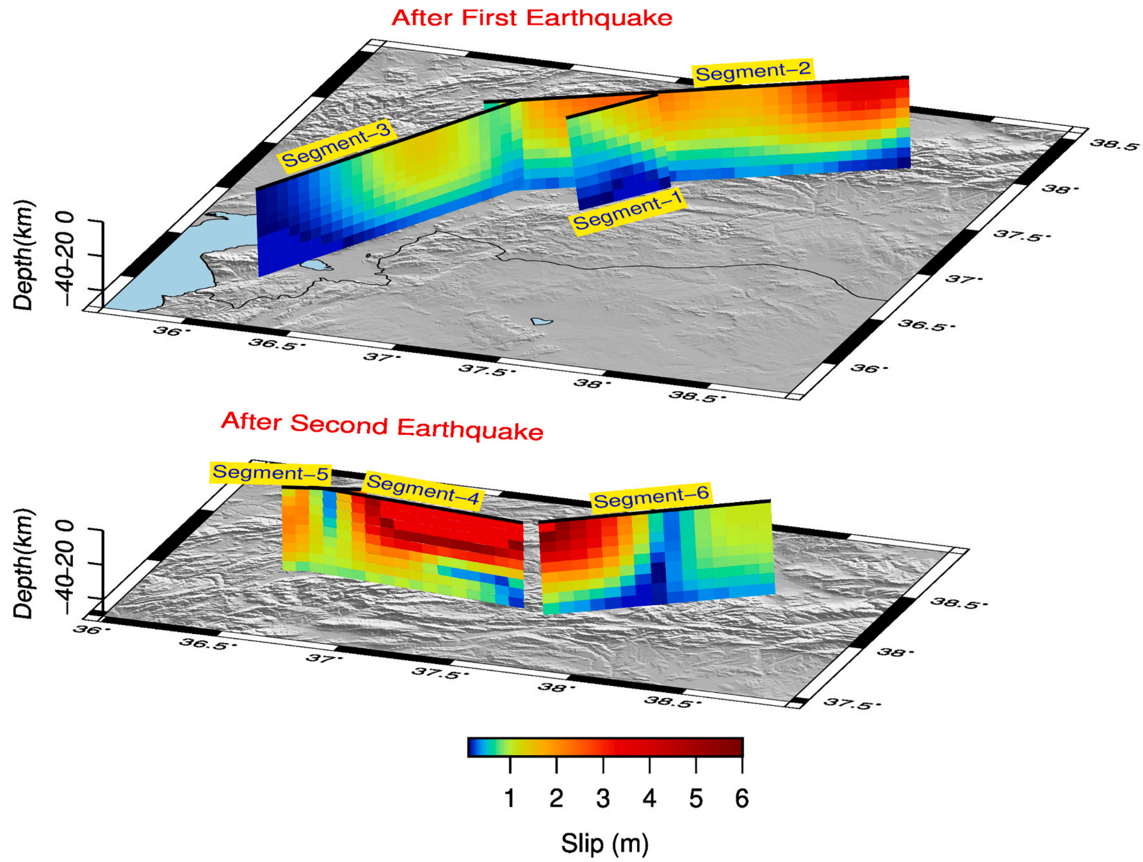

Fig. 8. The slip distributions calculated using only the co-seismic displacements of the first earthquake at 01.17 UTC Time (top) and only the second earthquake at 10.24 UTC (bottom).

individual slip distributions for the M_w 7.7 and M_w 7.6 earthquakes (Fig. 8). These permanent stations provide at least 20 days of GNSS data in total including the last 10 days within the pre-earthquake period. The co-seismic displacements at the permanent stations were separated by splitting the RINEX data file of February 6th into two sessions: the first session covering the first event time and the second session containing the second event time. While these individual solutions present a similar pattern of slip distribution, they are not identical.

Furthermore, Özkan et al. (2023) previously estimated the interseismic fully locking depths for Segment-2 and Segment-3 as 15 km and 7 km, respectively (Fig. S7). The co-seismic model in our study here verifies that the maximum slips on these segments align with the fully locking depths estimated during the interseismic phase (Fig. 7).

5. Discussion and conclusions

In this study, in order to investigate the co-seismic pattern of the earthquakes that occurred on February 06, 2023 in the vicinity of Kahramanmaraş, Turkey, a high-spatial-resolution GNSS network was established consisting of 113 sites including permanent GNSS stations and campaign observation sites. Afterwards, inverse modelling for surface displacements of a finite dislocation in an elastic half-space was implemented for the GNSS–derived co-seismic displacements estimated at the 113 sites. The inversion process consisted of two steps: the initial phase focused on modelling the fault geometry with uniform slip and the subsequent phase was assigned to estimate the slip vectors at the tiles of patches on the fault plane by fixing the fault geometry.

This study contains a unique geodetic dataset for southern Turkey that is not available anywhere else in terms of both spatial and temporal resolution. Apart from the dense structure of our GNSS network geometry, the temporal coverage of the network is also noteworthy to investigate strain accumulations on fault segments in the study region since most of the sites have an initial observation epoch in or before 2009. Thus, the EAFZ, DSFZ, KF, and KOF were investigated in detail in the previous studies (Aktug et al., 2016; Mahmoud et al., 2012; Özkan, 2021; Yıldız et al., 2020). The high seismic potentials of those fault segments were strongly emphasized, especially for the segments between Çelikhan and Türkoğlu on the EAFZ and KF between Türkoğlu and Antakya in the further south. In fact, Aktug et al. (2016) and Yıldız et al. (2020) have suggested magnitude of M_w 7.7 and M_w 7.2–7.6 for potential future earthquake on the EAFZ, respectively. At the moment, the fact that the major earthquakes in Kahramanmaraş have realized our predictions on February 06, 2023, it has shown how significant those studies are.

As with the determination of interseismic deformations, our motivation in this study was to demonstrate the capability of our GNSS network to provide highly accurate geodetic data in order to precisely determine the co-seismic displacements and successfully model the fault slip distributions after the recent devastating earthquakes in Kahramanmaraş. Our detailed analysis by this dense GNSS network prompted us to conclude that:

- In the aftermath of the Kahramanmaraş earthquakes on February 06, 2023, at 01.17 UTC Time (M_w 7.7 KOERI; M_w 7.9 USGS) and at 10.24 UTC Time (M_w 7.6 KOERI; M_w 7.5 USGS), the co-seismic displacements were ascertained across 113 sites. Of these, 73 sites were permanent GNSS stations, while, the remaining 40 sites were appropriate for campaign measurements.
- The co-seismic displacements were mostly compatible with the fault slip directions. The lateral co-seismic displacements in the study region have confirmed the dominant left-lateral slip directions along the EAFZ and its oblique branches. The east component of the GNSS

sites demonstrated relatively larger co-seismic displacements due to the fault strikes.
- The largest total displacements caused by these two major earthquakes were at the EKZ1, CRDK, and BNCA sites, with displacements of 466 cm, 362 cm, and 360 cm, respectively.
- The largest displacement among the east component for all sites was 464 cm at the EKZ1 site, which was only 7 km away from the epicentre of the earthquake on February 06, 2023, at 10.24 UTC Time. However, the most significant displacement among the north components for all sites was 277 cm at the FEVZ site, which was 42 km away from the epicentre of the earthquake on February 06, 2023, at 01.17 UTC Time.
- The vertical displacements were relatively smaller than the horizontal displacements by about 10–40 times, even at the sites closest to the epicentres of the two consecutive earthquakes.
- The first main shock (at 01.17 UTC Time) activated a rupture with three left-lateral slip patches connected to each other, namely 494 cm along EAFZ, 373 cm along Amanos Segment, and 152 cm along Narlı Segment. However, the fault mechanism on the Narlı segment, 45 km in length and dipping down to 10 km depth, was reverse slip of 141 cm.
- The main ruptures caused by the second main shock (at 10.24 UTC Time) were on the Çardak Fault with 391 cm left-lateral strike-slip and 141 cm normal slip, on the Doğanşehir Fault Zone with 407 cm left-lateral strike-slip and 52 cm normal slip, and on the Savrun Fault with 72 cm left-lateral strike-slip and 149 reverse slip.

Finally, the post-seismic deformations after these earthquakes and the transition to the interseismic phase, in which the strains on fault segments will accumulate, should be monitored by permanent GNSS stations and periodic campaign measurements, and the seismic modelling studies should be carried out to better understand the fault mechanisms in the vicinity of the study region.

CRediT authorship contribution statement

Ali Özkan: Writing – review & editing, Writing – original draft, Visualization, Software, Methodology, Investigation, Formal analysis. **Halil İbrahim Solak:** Writing – review & editing, Writing – original draft, Visualization, Software, Methodology, Investigation, Formal analysis. **İbrahim Tiryakioğlu:** Validation, Project administration, Investigation, Funding acquisition, Conceptualization. **Murat Doruk Şentürk:** Software, Formal analysis. **Bahadır Aktuğ:** Visualization, Validation, Software, Methodology, Formal analysis, Conceptualization. **Cemil Gezgin:** Writing – review & editing, Writing – original draft, Validation, Investigation. **Fatih Poyraz:** Validation, Investigation. **Hüseyin Duman:** Validation, Investigation. **Frédéric Masson:** Validation, Supervision, Conceptualization. **Göksu Uslular:** Writing – review & editing, Writing – original draft, Visualization. **Cemal Özer Yiğit:** Validation, Conceptualization. **Hasan Hakan Yavaşoğlu:** Validation, Supervision, Project administration, Funding acquisition, Conceptualization.

Declaration of Competing Interest

The authors declare the following financial interests/personal relationships which may be considered as potential competing interests:

Ibrahim Tiryakioglu reports financial support was provided by Scientific and Technological Research Council of Turkey. Hasan Hakan Yavasoglu reports financial support was provided by Istanbul Technical University.

Data availability

The data that has been used is confidential.

Acknowledgements

The authors would like to thank all participants who helped during the field studies. This article was supported financially by the Scientific and Technological Research Council of Turkey (TÜBİTAK) 1002-C Emergency Support Program for Field Study Focusing on Natural Disasters (project no. 123D005) and the Coordinator of Scientific Research Projects (BAP) of Istanbul Technical University (project no. MGA-2019-42243). We are much obliged to the Scientific and Technological Research Council of Turkey (TÜBİTAK), Disaster and Emergency Management Presidency (AFAD) and Adana-ASKİ for their support and providing archive GNSS data. The authors are grateful to anonymous reviewers for their helpful comments and valuable suggestions to improve the manuscript. The authors also thank Bünyamin Seven (Ülke Harita, Istanbul) for his support in data collection. For GPS data processing, the GAMIT/GLOBK software developed by Massachusetts Institute of Technology (MIT) was used (Herring et al., 2015a, 2015b). The GEODSUIT software was used for inverse modelling (Aktuğ et al., 2010). The GMT software was used to plot maps in this study (Wessel et al., 2013). The global dataset of active fault lines was obtained from the database of the GEM Global Active Faults project (Styron and Pagani, 2020). The authors are grateful to the journal and publisher for the publication support of our article as part of the Commitment to Inclusion and Diversity.

Appendix A. Supplementary data

Supplementary data to this article can be found online at https://doi.org/10.1016/j.tecto.2023.230041.

References

AFAD, 2023. 06 Şubat 2023 Pazarcık (Kahramanmaraş) Mw 7.7 ve Elbistan (Kahramanmaraş) Mw 7.6 Depremlerine İlişkin Ön Değerlendirme Raporu. The Disaster and Emergency Management Presidency, March, Istanbul.

Aktuğ, B., Kaypak, B., Çelik, R.N., 2010. Source parameters for the Mw = 6.6, 03 February 2002, Çay Earthquake (Turkey) and aftershocks from GPS, Southwestern Turkey. J. Seismol. 14, 445–456. https://doi.org/10.1007/s10950-009-9174-y.

Aktuğ, B., Dikmen, U., Dogru, A., Ozener, H., 2013. Seismicity and strain accumulation around Karliova Triple Junction (Turkey). J. Geodyn. 67, 21–29. https://doi.org/10.1016/j.jog.2012.04.008.

Aktug, B., Ozener, H., Dogru, A., Sabuncu, A., Turgut, B., Halicioglu, K., Yilmaz, O., Havazli, E., 2016. Slip rates and seismic potential on the East Anatolian Fault System using an improved GPS velocity field. J. Geodyn. 94–95, 1–12. https://doi.org/10.1016/j.jog.2016.01.001.

Alchalbi, A., Daoud, M., Gomez, F., McClusky, S., Reilinger, R., Romeyeh, M.A., Alsouod, A., Yassminh, R., Ballani, B., Darawcheh, R., Sbeinati, R., Radwan, Y., Al Masri, R., Bayerly, M., Al Ghazzi, R., Barazangi, M., 2010. Crustal deformation in northwestern Arabia from GPS measurements in Syria: Slow slip rate along the northern Dead Sea Fault. Geophys. J. Int. 180, 125–135. https://doi.org/10.1111/j.1365-246X.2009.04431.x.

Alp, H., Albora, A.M., Tur, H., 2011. A view of tectonic structure and gravity anomalies of Hatay Region Southern Turkey using wavelet analysis. J. Appl. Geophys. 75, 498–505. https://doi.org/10.1016/J.JAPPGEO.2011.07.004.

Ambraseys, N.N., 1989. Temporary seismic quiescence: SE Turkey. Geophys. J. Int. 96, 311–331. https://doi.org/10.1111/j.1365-246X.1989.tb04453.x.

Ambraseys, N.N., 2006. Comparison of frequency of occurrence of earthquakes with slip rates from long-term seismicity data: the cases of Gulf of Corinth, Sea of Marmara and Dead Sea Fault Zone. Geophys. J. Int. 165, 516–526. https://doi.org/10.1111/j.1365-246X.2006.02858.x.

Ambraseys, N.N., 2009. Earthquakes in the Mediterranean and Middle East: A Multidisciplinary Study of Seismicity up to 1900. Cambridge University Press.

Ambraseys, N.N., Jackson, J.A., 1998. Faulting associated with historical and recent earthquakes in the Eastern Mediterranean region. Geophys. J. Int. 133, 390–406.

Arpat, E., Şaroğlu, F., 1972. Some observations and thoughts on the East Anatolian fault. Bull. Miner. Res. Explor. Inst. Turk 73, 44–50.

Barka, A.A., Kadinsky-Cade, K., 1988. Strike-slip fault geometry in Turkey and its influence on earthquake activity. Tectonics 7, 663–684.

Bozkurt, E., 2001. Neotectonics of Turkey–a synthesis. Geodin. Acta 14, 3–30.

Bulut, F., Bohnhoff, M., Eken, T., Janssen, C., Kl, T., Dresen, G., 2012. The East Anatolian Fault Zone: Seismotectonic setting and spatiotemporal characteristics of seismicity based on precise earthquake locations. J. Geophys. Res. Solid Earth 117. https://doi.org/10.1029/2011JB008966.

Dewey, J.F., Hempton, M.R., Kidd, W.S.F., Saroglu, F., Şengör, A.M.C., 1986. Shortening of continental lithosphere: the neotectonics of Eastern Anatolia—a young collision zone. Geol. Soc. Lond. Spec. Publ. 19, 1–36.

Duman, T.Y., Emre, Ö., 2013. The east anatolian fault: geometry, segmentation and jog characteristics. Geol. Soc. Spec. Pub. 372, 495–529. https://doi.org/10.1144/SP372.14.

Faccenna, C., Bellier, O., Martinod, J., Piromallo, C., Regard, V., 2006. Slab detachment beneath eastern Anatolia: a possible cause for the formation of the North Anatolian fault. Earth Planet. Sci. Lett. 242, 85–97. https://doi.org/10.1016/j.epsl.2005.11.046.

Gülal, E., Erdoğan, H., Tiryakioğlu, İ., 2013. Research on the stability analysis of GNSS reference stations network by time series analysis. Digit. Signal Process. 23, 1945–1957.

Gülen, L., Barka, A., Toksöz, M.N., 1987. Continental collision and related complex deformation: Maras triple junction and surrounding structures, SE Turkey. Hacettepe Univ. Earth Sci. J. 14, 319–336.

Herring, T.A., King, R.W., Floyd, M.A., McClusky, S.C., 2015a. Global Kalman Filter VLBI and GPS Analysis Program. Massachusetts Institute of Technology, USA.

Herring, T.A., King, R.W., Floyd, M.A., McClusky, S.C., 2015b. Introduction to GAMIT/GLOBK. Massachusetts Institute of Technology, USA.

Hubert-Ferrari, A., King, G., Van Der Woerd, J., Villa, I., Altunel, E., Armijo, R., 2009. Long-term evolution of the North Anatolian Fault: new constraints from its eastern termination. Geol. Soc. Spec. Pub. 311, 133–154. https://doi.org/10.1144/SP311.5.

Hubert-Ferrari, A., Lamair, L., Hage, S., Schmidt, S., Çağatay, M.N., Avşar, U., 2020. A 3800 yr paleoseismic record (Lake Hazar sediments, eastern Turkey): implications for the East Anatolian Fault seismic cycle. Earth Planet. Sci. Lett. 538, 116152.

Jamason, P., Bock, Y., Fang, P., Gilmore, B., Malveaux, D., Prawirodirdjo, L., Scharber, M., 2004. SOPAC Web site (http://sopac.ucsd.edu). GPS Solutions 8, 272–277. https://doi.org/10.1007/s10291-004-0118-2.

Karig, D.E., Kozlu, H., 1990. Late Palaeogene-Neogene evolution of the triple junction region near Maraş, south-central Turkey. J. Geol. Soc. London 147, 1023–1034. https://doi.org/10.1144/gsjgs.147.6.1023.

Kiratzi, A.A., 1993. A study on the active crustal deformation of the north and east anatolian fault zones. Tectonophysics 225, 191–203. https://doi.org/10.1016/0040-1951(93)90279-S.

Kirkpatrick, S., Gelatt Jr., C.D., Vecchi, M.P., 1983. Optimization by simulated annealing. Science 220, 671–680.

Koçyiğit, A., Yilmaz, A., Adamia, S., Kuloshvili, S., 2001. Neotectonics of East Anatolian Plateau (Turkey) and lesser caucasus: implication for transition from thrusting to strike-slip faulting. Geodin. Acta 14, 177–195. https://doi.org/10.1080/09853111.2001.11432443.

KOERI, 2023. 06 Şubat 2023 Gaziantep-Kahramanmaraş ve 20 Şubat 2023 Hatay Depremleri Ön Değerlendirme Raporu. Kandilli Rasathanesi ve Deprem Araştırma Enstitüsü, İstanbul.

Kurt, A.İ., Özbakır, A.D., Cingöz, A., Ergintav, S., Doğan, U., Özarpacı, S., 2023. Contemporary velocity field for Turkey inferred from combination of a dense network of long term GNSS observations. Turk. J. Earth Sci. 32, 275–293.

Lyberis, N., Yurur, T., Chorowicz, J., Kasapoglu, E., Gundogdu, N., 1992. The East Anatolian Fault: an oblique collisional belt. Tectonophysics 204, 1–15.

Mahmoud, Y., Masson, F., Meghraoui, M., Cakir, Z., Alchalbi, A., Yavasoglu, H., Yönlü, O., Daoud, M., Ergintav, S., Inan, S., 2012. Kinematic study at the junction of the east anatolian fault and the dead sea fault from GPS measurements. J. Geodyn. 67, 30–39. https://doi.org/10.1016/j.jog.2012.05.006.

Meghraoui, M., Cakir, Z., Masson, F., Mahmood, Y., Ergintav, S., Alchalbi, A., Inan, S., Daoud, M., Yonlu, O., Altunel, E., 2011. Kinematic modelling at the triple junction between the Anatolian, Arabian, African plates (NW Syria and in SE Turkey). Geophys. Res. Abstr. 13, 12599.

Melgar, D., Taymaz, T., Ganas, A., Crowell, B.W., Öcalan, T., Kahraman, M., Tsironi, V., Yolsal-Çevikbilen, S., Valkaniotis, S., Irmak, T.S., Eken, T., Erman, C., Özkan, B., Doğan, A.H., Altuntaş, C., 2023. Sub-and super-shear ruptures during the 2023 Mw 7.8 and Mw 7.6 earthquake doublet in SE Türkiye. Seismica 2.

Okada, Y., 1985. Surface deformation due to shear and tensile faults in a half-space. Bull. Seismol. Soc. Am. 75, 1135–1154.

Özkan, A., 2021. Determination of the kinematics of active faults in the Northeastern Mediterranean region by GPS observations and elastic half-space dislocation model. Doctoral dissertation. Istanbul Technical University, Graduate School, Istanbul.

Özkan, A., Yavaşoğlu, H.H., Masson, F., 2023. Present-day strain accumulations and fault kinematics at the Hatay Triple Junction using new geodetic constraints. Tectonophysics 854, 229819.

Reilinger, R.E., McClusky, S.C., Oral, M.B., King, R.W., Toksoz, M.N., Barka, A.A., Kinik, I., Lenk, O., Sanli, I., 1997. Global Positioning System measurements of present-day crustal movements in the Arabia-Africa-Eurasia plate collision zone. J. Geophys. Res. Solid Earth 102, 9983–9999. https://doi.org/10.1029/96jb03736.

Reilinger, R., McClusky, S., Vernant, P., Lawrence, S., Ergintav, S., Cakmak, R., Ozener, H., Kadirov, F., Guliev, I., Stepanyan, R., Nadariya, M., Hahubia, G., Mahmoud, S., Sakr, K., ArRajehi, A., Paradissis, D., Al-Aydrus, A., Prilepin, M., Guseva, T., Evren, E., Dmitrotsa, A., Filikov, S.V., Gomez, F., Al-Ghazzi, R., Karam, G., 2006. GPS constraints on continental deformation in the Africa-Arabia-Eurasia continental collision zone and implications for the dynamics of plate interactions. J. Geophys. Res. Solid Earth 111, 1–26. https://doi.org/10.1029/2005JB004051.

Rojay, B., Heimann, A., Toprak, V., 2001. Neotectonic and volcanic characteristics of the Karasu fault zone (Anatolia, Turkey): the transition zone between the Dead Sea transform and the East Anatolian fault zone. Geodin. Acta 14, 197–212.

Saroglu, F., Emre, O., Kuscu, I., 1992. The East Anatolian Fault Zone of Turkey. Ann. Tecton. Special Issue, VI 99–125.

Sbeinati, M.R., Darawcheh, R., Mouty, M., 2005. The historical earthquakes of Syria: an analysis of large and moderate earthquakes from 1365 B.C. to 1900 A.D. Ann. Geophys. 48, 347–435. https://doi.org/10.4401/ag-3206.

Şengör, A.M.C., Yılmaz, Y., 1981. Tethyan evolution of Turkey: a plate tectonic approach. Tectonophysics 75. https://doi.org/10.1016/0040-1951(81)90275-4.

Sengor, A.M.C., Gorur, N., Saroglu, F., 1985. Strike slip faulting and related basin formation in zones of tectonic escape: Turkey as a case study. In: Biddle, K.T., Christie-Blick, N. (Eds.), Strike Slip Deformation, Basin Formation, and Sedimentation, 37, pp. 227–264.

Şengör, A.M.C., Zabcı, C., Natal'in, B.A., 2018. Continental transform faults: congruence and incongruence with normal plate kinematics. In: Transform Plate Boundaries and Fracture Zones. Elsevier, pp. 169–247. https://doi.org/10.1016/B978-0-12-812064-4.00009-8.

Styron, R., Pagani, M., 2020. The GEM global active faults database. Earthq. Spectra 36, 160–180. https://doi.org/10.1177/8755293020944182.

Tatar, O., Piper, J.D.A., Gürsoy, H., Heimann, A., Koçbulut, F., 2004. Neotectonic deformation in the transition zone between the Dead Sea Transform and the East Anatolian Fault Zone, Southern Turkey: a palaeomagnetic study of the Karasu Rift Volcanism. Tectonophysics 385, 17–43. https://doi.org/10.1016/j.tecto.2004.04.005.

Taymaz, T., Eyidoğan, H., Jackson, J., 1991. Source parameters of large earthquakes in the East Anatolian Fault Zone (Turkey). Geophys. J. Int. 106, 537–550. https://doi.org/10.1111/j.1365-246X.1991.tb06328.x.

Tiryakioğlu, İ., Floyd, M., Erdoğan, S., Gülal, E., Ergintav, S., McClusky, S., Reilinger, R., 2013. GPS constraints on active deformation in the Isparta Angle region of SW Turkey. Geophys. J. Int. 195, 1455–1463.

Tiryakioglu, I., Yavasoglu, H., Ugur, M.A.U., Ozkaymak, C., Yilmaz, M., Kocaoglu, H., Turgut, B., 2017a. Analysis of October 23 (Mw 7.2) and November 9 (Mw 5.6), 2011 Van earthquakes using long-term GNSS time series. Earth Sci. Res. J. 21, 147–156. https://doi.org/10.15446/esrj.v21n3.62812.

Tiryakioglu, I., Yigit, C.O., Yavasoglu, H., Saka, M.H., Alkan, R.M., 2017b. The determination of interseismic, coseismic and postseismic deformations caused by the Gökçeada-Samothraki earthquake (2014, Mw: 6.9) based on GNSS data. J. Afr. Earth Sci. 133, 86–94.

Tiryakioğlu, Aktuğ, B., Yiğit, C., Yavaşoğlu, H.H., Sozbilir, H., Özkaymak, Poyraz, F., Taneli, E., Bulut, F., Doğru, A., Özener, H., 2018. Slip distribution and source parameters of the 20 July 2017 Bodrum-Kos earthquake (Mw6.6) from GPS observations. Geodin. Acta 30, 1–14. https://doi.org/10.1080/09853111.2017.1408264.

U.S. Geological Survey, 2023a. Event Page for the M 7.8 - Pazarcik Earthquake, Kahramanmaras Earthquake Sequence. https://earthquake.usgs.gov/earthquakes/eventpage/us6000jllz/ last accessed March 5, 2023.

U.S. Geological Survey, 2023b. Event Page for the M 7.5 - Elbistan Earthquake, Kahramanmaras Earthquake Sequence. https://earthquake.usgs.gov/earthquakes/eventpage/us6000jlqa/ last accessed March 5, 2023.

Wang, L., Wang, R., Roth, F., Enescu, B., Hainzl, S., Ergintav, S., 2009. Afterslip and viscoelastic relaxation following the 1999 M 7.4 Izmit earthquake from GPS measurements. Geophys. J. Int. 178, 1220–1237.

Wessel, P., Smith, W.H.F., Scharroo, R., Luis, J.F., Wobbe, F., 2013. GMT 5: A major new release of the Generic Mapping Tools. Eos Trans. AGU 94, 409–410.

Westaway, R., 1994. Present-day kinematics of the Middle East and eastern Mediterranean. J. Geophys. Res. Solid Earth 99, 12071–12090.

Westaway, R., 2003. Kinematics of the Middle East and Eastern Mediterranean updated. Turk. J. Earth Sci. 12, 5–46.

Westaway, R., Arger, J., 1996. The Gölbaşi basin, southeastern Turkey: a complex discontinuity in a major strike-slip fault zone. J. Geol. Soc. London 153, 729–744. https://doi.org/10.1144/gsjgs.153.5.0729.

Yavasoglu, H.H., Tiryakioglu, I., Karabulut, M.F., Eyubagil, E.E., Ozkan, A., Masson, F., Klein, E., Gulal, V.E., Alkan, R.M., Alkan, M.N., Isiler, M., Arslan, A.E., 2021. New geodetic constraints to reveal seismic potential of central marmara region, Turkey. Bull. Geophys. Oceanogr. 62, 513–526. https://doi.org/10.4430/bgta0351.

Yıldız, S.S., Özkan, A., Yavaşoğlu, H.H., Masson, F., Tiryakioğlu, İ., Alkan, M.N., Bilgi, S., 2020. Determination of recent tectonic deformations in the vicinity of Adana–Osmaniye–Hatay–Gaziantep triple junction region by half-space modeling. Compt. Rend. Géosci. 352, 225–234.